Focused electron beam induced deposition as a tool to create electron vortices

Focused electron beam induced deposition as a tool to create electron vortices

A. Béché[a], R. Winkler[b], H. Plank[b,c], F. Hofer[c], J. Verbeeck[a]

[a] *EMAT, University of Antwerp, Groenenborgerlaan 171, 2020 Antwerp, Belgium*
[b] *Graz Centre for Electron Microscopy, Steyrergasse 17, 8010 Graz, Austria*
[c] *Institute for Electron Microscopy and Nanoanalysis, Graz University of Technology, Steyrergasse 17, A-8010 Graz, Austria*

Abstract

Focused electron beam induced deposition (FEBID) is a microscopic technique that allows geometrically controlled material deposition with very high spatial resolution. This technique was used to create a spiral aperture capable of generating electron vortex beams in a transmission electron microscope (TEM). The vortex was then fully characterized using different TEM techniques estimating the average orbital angular momentum to be $\sim 0.8\hbar$ per electron with almost 60% of the beam ending up in the $\ell = 1$ state.

Keywords: Focused electron beam induced deposition (FEBID), Transmission electron microscope (TEM), Vortex, Holography.

1. Introduction

The recent discovery of electron vortex beams (Uchida and Tonomura, 2010; Verbeeck et al., 2010; McMorran et al., 2011) in transmission electron microscopy (TEM) and their application in nanoparticle manipulation (Verbeeck et al., 2013), chiral structure determination (Juchtmans et al., 2015) and atomically resolved magnetic mapping (Rusz and Bhowmick, 2013) drive an increasing interest in producing efficient and custom electron phase plates. Indeed, high intensity vortex beams with perfectly controlled orbital angular momentum are a key requirement to extract magnetic information down to the atomic scale. En route to creating the most efficient vortex generating phase plate, numerous methods have been investigated. Based on light optics, holographic reconstruction gratings (Verbeeck et al., 2010; McMorran et al., 2011) were shown to be a convenient way of reliably creating near pure orbital angular momentum (OAM) states. This method however has the disadvantage of inefficiency (maximum 25% of the electrons end up in the desired state (Grillo et al., 2014; Harvey et al., 2014)) and suffers from the creation of unwanted side-beams (Pohl et al., 2015). Mode converter methods have also been proposed as electron vortex generators but the realization of good experimental setup remains challenging (Schattschneider et al., 2012). The use of a probe corrector as a phase manipulation tool (Clark et al., 2013) was shown to allow for great flexibility but gives rise to less pure OAM states, while also being far from efficient due to the use of a thin annular aperture blocking most of the electrons. Magnetic needle based phase plates seem to solve most of these issues, providing single, pure OAM beams with near 100% efficiency (Béché et al., 2014; Blackburn and Loudon, 2014).

In this paper however, we will deal with an alternative way of producing electron vortex beams based on the phase shift induced by interaction of an electron beam with matter. This phase shift can be expressed $\Delta\Phi = C_E \int_0^t V_E(r,z)dz$, where $C_E = \frac{2\pi e}{\lambda}\frac{E+E_0}{E(E+2E_0)}$ is the interaction constant depending on the energy E of the incoming electron beam and its rest energy E_0, λ the electron wave length and V_E the mean

* *Email address:* armand.beche@uantwerpen.be (A. Béché)

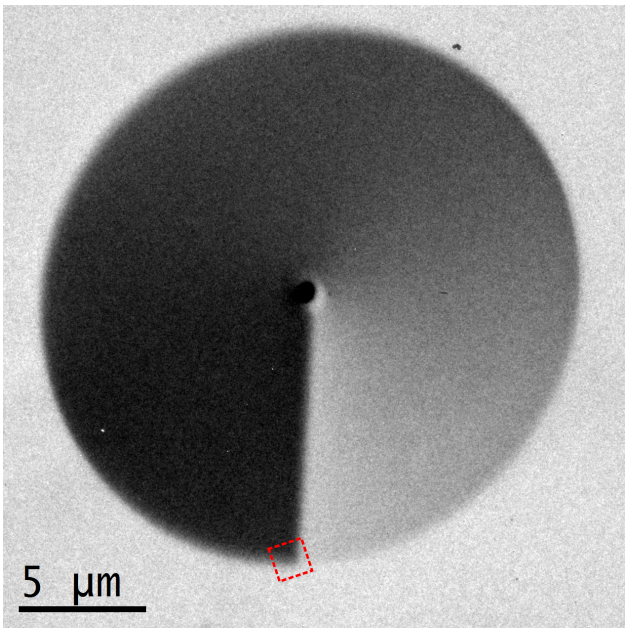

Figure 1: *TEM overview image of the spiral phase plate. The black center point corresponds to the Pt center, blocking the unwanted central beam.*

inner potential of the material. In order to create an electron vortex beam, of typical form $\Psi(r, \phi, z) = A(r)\exp(i\ell\phi)\exp(ikz)$, with $\ell \neq 0$ the topological charge of the beam (Bliokh et al., 2007), one needs to create a phase plate with a spiraling geometry. The first ever observed electron vortex beam was obtained this way by Uchida and Tonomura (Uchida and Tonomura, 2010) based on a fortunate stacking of graphite plates. The idea was then extended to custom shaped spiral phase plates using a focused ion beam (FIB) microscope (Shiloh et al., 2014). In this paper, we want to further investigate the possibility of making a spiral phase plate with focused electron beam induced deposition (Utke et al., 2008, 2012; Winkler et al., 2015) to act as a vortex beam generator. The technique offers versatility in terms of aperture geometry, size and composition.

2. Experimental settings

2.1. Samples

In order to limit absorption of the electron beam, an ultrathin (8 nm) silicon-nitride window grid was used as a substrate to fabricate a silicon oxide spiral phase plate with a diameter of 20 μm. Silicon oxide was chosen for its relatively low density, thus limiting the absorption of the phase plate as well as allowing sufficient precision in the deposited thickness. The deposition of SiO_2 via a precursor (TEOS, Tetraethyl orthosilicate) occurs under the electron beam of a dual-beam instrument (FEI Nova 200) operating at 5 kV with 6.10^{-5} mbar pressure and a beam current of 1.6 nA (spot size of $\simeq$ 50 nm). The final aperture shape was realized from a bitmap converted into a stream file, the beam following a serpentine strategy for a series of 200 passes with a 10 μs dwell time. In order to make sure the central part of the aperture does not introduce an unwanted component with zero OAM, it was filled with platinum (deposited from $MeCpPt(IV)Me_3$) in sufficient quantity to block the incoming electron beam. In order to properly check the efficiency of the aperture, it was placed in the Qu-An-TEM microscope, an FEI double Cs corrected microscope operating at 300 kV in Lorentz mode. This mode is required to provide sufficient field of view and spatial coherence over the diameter of the phase plate. In order to quantify the phase jump generated by the step in the spiral phase plate, electron holography is performed, making use of a Möllenstedt biprism operating at 180 V. A

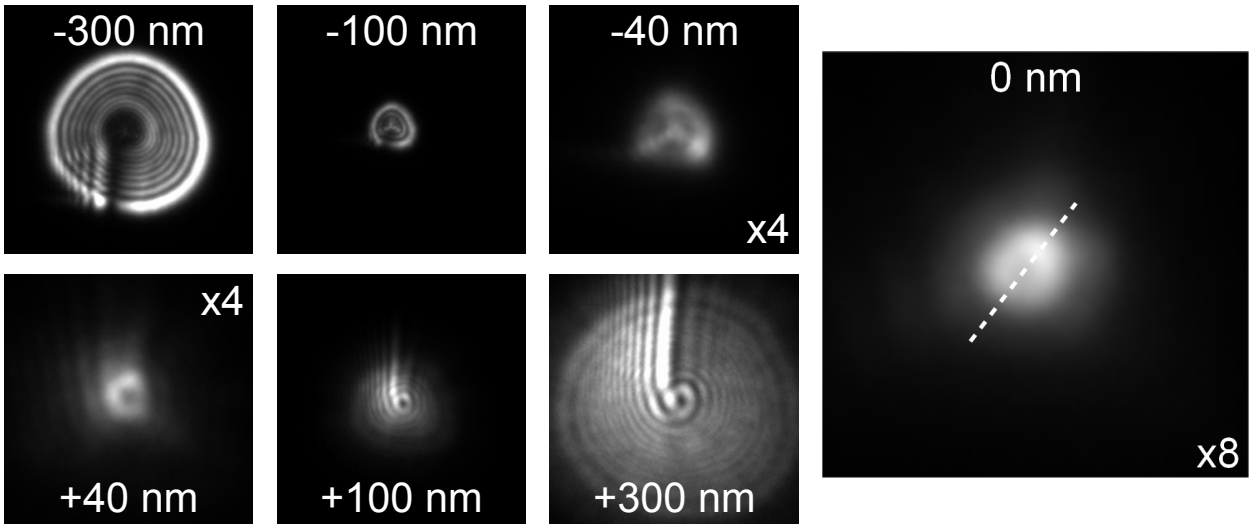

Figure 2: *Through focus series in the far field plane of the spiral phase plate. The dotted line corresponds to a line profile displayed in Figure 6.*

bright field TEM picture of the aperture is displayed in Figure 1. In order to overcome severe charging issues leading to dramatic aberrations of the electron beam, a thin layer of carbon (10 to 20 nm) was deposited on the surface. This conductive layer prevents charge buildup at the surface of the sample, which otherwise strongly affect the total phase shift.

3. OAM characterization

A vortex probe is produced in the far field of the aperture plane which, in this case, corresponds to the diffraction plane, as the aperture is located in the sample plane. An ideal vortex probe should display the typical doughnut-like intensity distribution of a vortex, with a bright ring and a dark central part that does not disappear upon defocusing. This dark center arises from destructive interference along the propagation axis of the vortex, when all phases meet together. Accordingly, a through-focus series of the probe was recorded and is displayed in Figure 2.

One can see the typical vortex profile even when the probe is fully focused (a line profile is displayed in Figure 6). However, on the negative focus side, it seems the dark central spot vanishes and is replaced by a caustic spot. Furthermore, the central interference region for similar over and under-focus values shows different sizes. These behaviors were attributed to remaining charges at the surface of the spiral phase plate which act in two ways. On the one hand, they add extra aberrations to the electron beam, and make the three fold astigmatism caustic visible. On the other hand, the surface charges globally act as an electrostatic monopole similar to a (de)focussing electrostatic lens. The presence of charges was experimentally obvious as, upon first introduction in the microscope, the phase plate was not carbon coated. The amount of aberrations was such that it was impossible to focus the probe in the far field mode. Just displacing the sample out of the field of view was then sufficient to retrieve a normal beam. Covering the phase plate with carbon then alleviated the situation but some aberrations remain present.

The absence of a scale bar in Figure 2 is deliberate as such an aperture is not meant to be used in the sample plane but either in a condenser, an objective or a selected area aperture plane. In the present case, the only value physically relevant would have been angles as the probe is imaged in the far field plane of the Lorentz lens. However, the Lorentz mode is almost impossible to calibrate in diffraction as the convergence angle of the beam is very small and the camera length values are extremely high. As error bars would be high, we decided to leave the image uncalibrated.

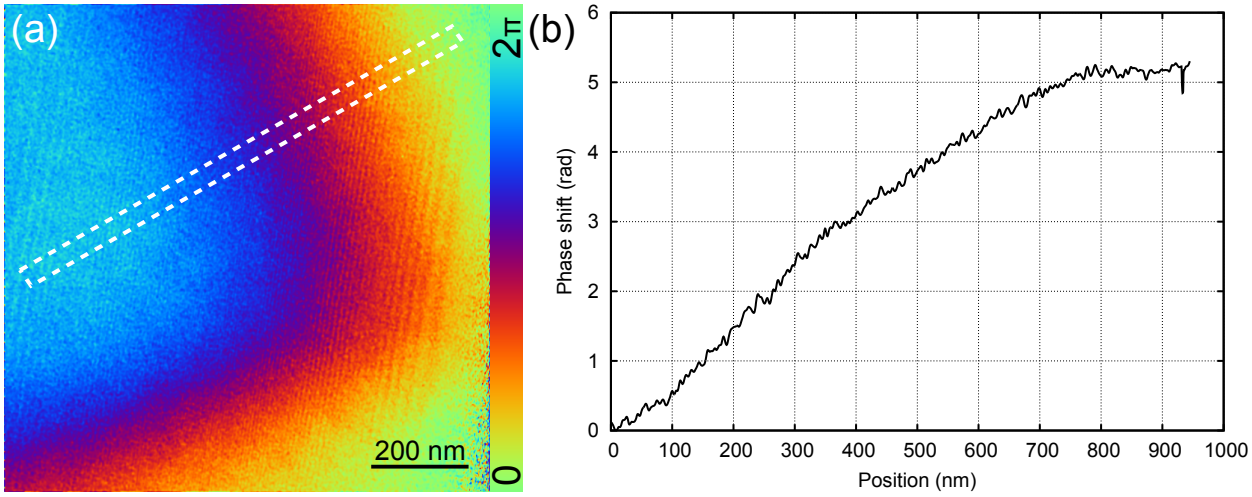

Figure 3: *(a) Reconstructed hologram mapping the difference in phase shift at the edge of the spiral aperture, marked as a red square in Figure 1. (b) Line profile showing the phase shift evolution between the lowest point and the highest point of the aperture.*

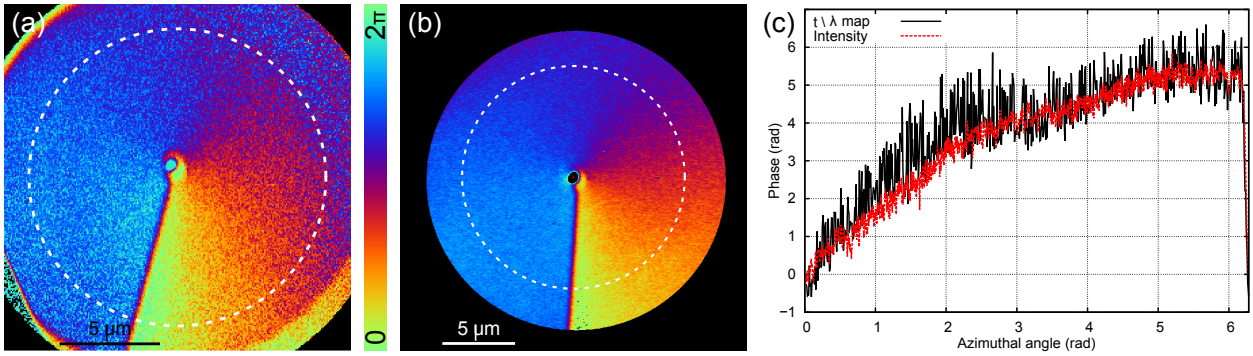

Figure 4: *(a) Phase map calculated from a $t \setminus \lambda$. (b) Phase map calculated from the intensity map displayed in Figure 1. (c) Comparison of circular profiles extracted from (a) and (b) on the dotted lines.*

To further quantify the total phase shift induced by the aperture, electron holography was performed at the step part of the spiral. Upon interference of electrons that passed through the thickest and thinnest parts of the phase plate, one can have a direct measurement of the phase shift induced by the aperture step after holographic reconstruction (Lichte, 1986). Such a reconstructed hologram is displayed in Figure 3, together with a line profile extracted from the lowest phase shift position to the highest one. The total phase shift was estimated to be 5.1 rad, corresponding to a total orbital angular momentum of $< \ell > \sim 0.8$. The ramp profile of the phase appears because of the slowly increasing thickness at the spiral edge, mainly due to the size of the FEBID probe and some remaining experimental drift during the aperture growth.

The holography results gave access to the phase jump at the step part of the aperture, but a full phase map of the aperture would be of more interest, especially to calculate an OAM decomposition profile. Unfortunately, the maximum field of view available in holography is too narrow to properly map the entire aperture over the 20 μm range. One of the best ways to reconstruct the phase over the full aperture would be to measure the thickness of the spiral phase plate, as it directly scales with the phase via the mean inner potential. Even a relative measurement will be sufficient as the phase jump has been quantified by holography. Typical t/λ maps acquired by EELS can provide such information but again, the field of view

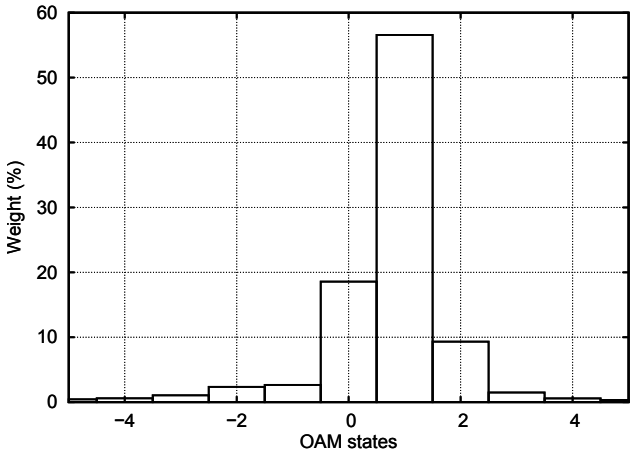

Figure 5: *OAM decomposition of the electron wave after interaction with the spiral phase plate.*

in the TEM is too narrow to properly map the entire object. Another alternative is to make use of the intensity map of Figure 1 that scales with the sample thickness for weak phase object approximation. In order to check that this hypothesis was realistic, we acquired a t/λ map at the center of the spiral phase plate and transformed it into a phase map, as displayed in Figure 4(a). The exact same operation was applied on the intensity map (Figure 4(b)). Circular profiles taken at identical positions in both images were then compared in Figure 4(c), and appear to be very similar. The noise level in the t/λ based phase profile is much higher than the one based on the intensity due to the much lower signal to noise ratio offered by the EELS technique. Now that the phase map can be reconstructed from the intensity image with good approximation, we can decompose it into OAM eigenstates $a_m = \frac{1}{\sqrt{2\pi}} \int_0^{2\pi} \exp(-im\phi)\Psi(\phi)d\phi$ (Molina-Terriza et al., 2001; Berkhout et al., 2011). The result of such decomposition is presented in Figure 5, where almost 60% of the beam ends up in the $\ell = 1$ state and the rest is mainly scattered in the $\ell = 0$ and $\ell = 2$ states.

4. Discussion

In addition to the OAM decomposition, the reconstructed phase map can be used to simulate the propagation of the wave impinging the spiral phase plate up to the far field plane. In order to be as close to the experiment as possible, the aberration function of the microscope was included in the Fresnel propagator. Moreover, as the projected size of the probe on the GIF CCD was only a dozen of pixels at the highest magnification available, the modulation transfer function (MTF) of the camera was introduced to take into account the signal blurring during the data acquisition (Van den Broek et al., 2012). An estimate of the amplitude contrast can be obtained from the intensity image leading to a maximum amplitude change of $\simeq 0.6$. Adding this amplitude contrast to the simulated probe profile however only marginally affects the profile.

A reproduction of the experimental through focus series was first calculated and is displayed in Figure 6. The best fit to the experimental series was obtained introducing a three fold astigmatism of $A_2 = 20\ mm$ and a spherical aberration value of $C_s = 800\ m$. These aberrations are at least a 100 times higher than expected in the standard Lorentz mode, and are generated by the presence of remaining charges at the surface of the aperture. However, the effects of charging could not be reproduced exactly. The presence of the three fold caustic in the -100 nm defocus case could only be reproduced for an A_2 value twice as high, leading to a very triangular form of the probe, not visible experimentally. And the unexpectedly large dark center in the -300 nm image is not present in the simulations. These deviations are caused by the

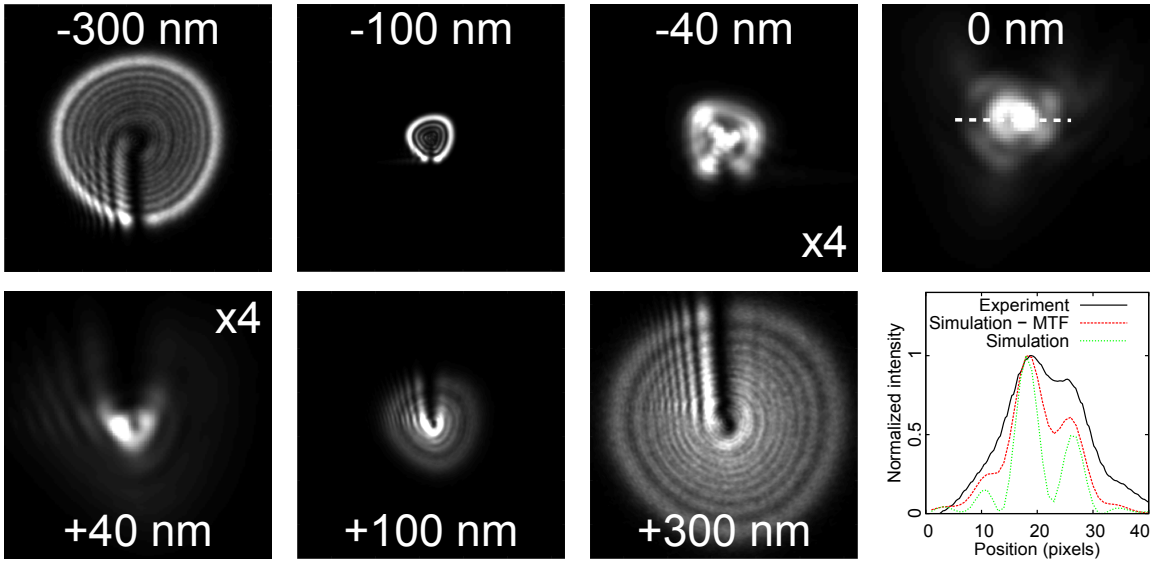

Figure 6: *Simulated through focus series of the far field plane of the spiral aperture reproducing the experimental one displayed in Figure 2. A graph compares the line profiles of the focused probe in the experimental case and the simulated cases with and without taking into account the MTF of the camera.*

actual charge distribution that differs from the simplified model that takes into account only the dominant aberration orders.

Further investigation of the focused probe was also possible thanks to the simulations. In the graph of Figure 6, profiles were extracted from the focused probe in three cases: the experimental image and the simulated images with and without taking into account the MTF of the GIF CCD. In the latter case, the intensity step of the vortex core almost reaches zero, as expected for a phase discontinuity. The effect of the MTF on the vortex is clearly visible as the dark center is filled up to 50%. However, the MTF effect does not fully explain the even more filled center of the experimental case. One can observe that in addition to the filling of the dark vortex core, the width of the overall vortex is also increased. The scattering of the amorphous SiO_2 composing the phase plate is not likely to be the cause of the vortex probe blurring as it happens at angles much larger than the probe convergence angle. Most likely, the observed blurring effect is induced by the remaining vibrations of the electron beam or by the effect of the electron source size broadening.

From the above results, the FEBID technique proved to be an efficient way of creating a spiral phase plate with the expected characteristics. One could argue about the requirement of the Pt island in the middle of the aperture, originally designed to block unwanted scattering from the unfilled center of the phase plate, as its contribution in terms of surface is almost negligible (less than 0.2%). Using the numerical model of the spiral phase plate, it was possible to simulate the phase plate response with and without the presence of the Pt island, showing its effect to be indeed negligible.

However, as the phase shift comes from the electron-matter interaction, the spiral phase plate only provides the correct phase shift at a given acceleration voltage. For microscopes operating at different acceleration voltages, the need for multiple apertures could pose experimental restrictions. During operation, contamination can appear which can charge, again leading to a problematic influence on the phase plate. This can be limited in modern TEMs thanks to improved vacuum design and proper cold traps. On the upside, phase plates like this provide a local definition of the phase over an aperture, while most other techniques try to influence the phase by controlling electrostatic or magnetic fields from the boundary of the aperture, offering only limited freedom in the obtained phase plate.

The high spatial resolution offered by the FEBID technique allows the realization of more complex phase

plates, such as the Zernike or Hilbert types (Nagayama, 2011). Moreover, a wide variety of materials can be deposited, insulating or conductive, magnetic or not, the potential applications being only limited by the imagination of the user.

5. Conclusion

In this paper, we demonstrated a silicon oxide spiral aperture created using FEBID which successfully generated an electron vortex beam upon interaction with the incoming electron beam of a TEM with an average orbital angular momentum of $< \ell > \sim 0.8$ and almost 60% of the beam ending in the $\ell = 1$ state. The FEBID technique is thus proven to be an efficient technique to create versatile apertures and phase plates for TEM with both advantages and drawbacks.

6. Acknowledgements

A.B and J.V. acknowledge funding from the European Research Council under the 7th Framework Program (FP7), ERC Starting Grant No. 278510 VORTEX. J.V., R.W., H.P. and F.H. acknowledge financial support from the European Union under the 7th Framework Program (FP7) under a contract for an Integrated Infrastructure Initiative (Reference No. 312483 ESTEEM2). R.W and H.P also acknowledge financial support by the COST action CELINA (Nr. CM1301) and the EUROSTARS project TRIPLE-S (Nr. E!8213). The Qu-Ant-EM microscope was partly funded by the Hercules fund from the Flemish Government.

7. References

Béché, A., Van Boxem, R., Van Tendeloo, G., and Verbeeck, J. (2014). Magnetic monopole field exposed by electrons. *Nature Physics*, 10(1):26–29.

Berkhout, G. C. G., Lavery, M. P. J., Padgett, M. J., and Beijersbergen, M. W. (2011). Measuring orbital angular momentum superpositions of light by mode transformation. *Optics Letters*, 36(10):1863.

Blackburn, A. M. and Loudon, J. C. (2014). Vortex beam production and contrast enhancement from a magnetic spiral phase plate. *Ultramicroscopy*, 136:127–143.

Bliokh, K. Y., Bliokh, Y. P., Savelev, S., and Nori, F. (2007). Semiclassical Dynamics of Electron Wave Packet States with Phase Vortices. *Physical Review Letters*, 99(19):190404.

Clark, L., Béché, A., Guzzinati, G., Lubk, A., Mazilu, M., Van Boxem, R., and Verbeeck, J. (2013). Exploiting Lens Aberrations to Create Electron-Vortex Beams. *Physical Review Letters*, 111(6):064801.

Grillo, V., Gazzadi, G. C., Karimi, E., Mafakheri, E., Boyd, R. W., and Frabboni, S. (2014). Highly efficient electron vortex beams generated by nanofabricated phase holograms. *Applied Physics Letters*, 104(4):043109.

Harvey, T. R., Pierce, J. S., Agrawal, A. K., Ercius, P., Linck, M., and McMorran, B. J. (2014). Efficient diffractive phase optics for electrons. *New Journal of Physics*, 16(9):093039.

Juchtmans, R., Béché, A., Abakumov, A., Batuk, M., and Verbeeck, J. (2015). Using electron vortex beams to determine chirality of crystals in transmission electron microscopy. *Physical Review B*, 91(9):094112.

Lichte, H. (1986). Electron holography approaching atomic resolution. *Ultramicroscopy*, 20(3):293–304.

McMorran, B. J., Agrawal, A., Anderson, I. M., Herzing, A. A., Lezec, H. J., McClelland, J. J., and Unguris, J. (2011). Electron Vortex Beams with High Quanta of Orbital Angular Momentum. *Science*, 331(6014):192–195.

Molina-Terriza, G., Torres, J. P., and Torner, L. (2001). Management of the Angular Momentum of Light: Preparation of Photons in Multidimensional Vector States of Angular Momentum. *Physical Review Letters*, 88(1):013601.

Nagayama, K. (2011). Another 60 years in electron microscopy: development of phase-plate electron microscopy and biological applications. *Journal of Electron Microscopy*, 60 Suppl 1:S43–62.

Pohl, D., Schneider, S., Rusz, J., and Rellinghaus, B. (2015). Electron vortex beams prepared by a spiral aperture with the goal to measure EMCD on ferromagnetic films via STEM. *Ultramicroscopy*, 150:16–22.

Rusz, J. and Bhowmick, S. (2013). Boundaries for Efficient Use of Electron Vortex Beams to Measure Magnetic Properties. *Physical Review Letters*, 111(10):105504.

Schattschneider, P., Stger-Pollach, M., and Verbeeck, J. (2012). Novel Vortex Generator and Mode Converter for Electron Beams. *Physical Review Letters*, 109(8):084801.

Shiloh, R., Lereah, Y., Lilach, Y., and Arie, A. (2014). Sculpturing the electron wave function using nanoscale phase masks. *Ultramicroscopy*, 144:26–31.

Uchida, M. and Tonomura, A. (2010). Generation of electron beams carrying orbital angular momentum. *Nature*, 464:737–739.

Utke, I., Hoffmann, P., and Melngailis, J. (2008). Gas-assisted focused electron beam and ion beam processing and fabrication. *Journal of Vacuum Science & Technology B*, 26(4):1197–1276.

Utke, I., Moshkalev, S., and Russell, P. (2012). *Nanofabrication Using Focused Ion and Electron Beams: Principles and Applications*. Oxford University Press.

Van den Broek, W., Van Aert, S., and Van Dyck, D. (2012). Fully Automated Measurement of the Modulation Transfer Function of Charge-Coupled Devices above the Nyquist Frequency. *Microscopy and Microanalysis*, 18(02):336–342.

Verbeeck, J., Tian, H., and Schattschneider, P. (2010). Production and application of electron vortex beams. *Nature*, 467:301–304.

Verbeeck, J., Tian, H., and Van Tendeloo, G. (2013). How to Manipulate Nanoparticles with an Electron Beam? *Advanced Materials*, 25(8):1114–1117.

Winkler, R., Szkudlarek, A., Fowlkes, J. D., Rack, P. D., Utke, I., and Plank, H. (2015). Toward Ultraflat Surface Morphologies During Focused Electron Beam Induced Nanosynthesis: Disruption Origins and Compensation. *ACS Applied Materials & Interfaces*, 7(5):3289–3297.